Stem Cell Reports
Article

OPEN ACCESS

Quantified F-Actin Morphology Is Predictive of Phagocytic Capacity of Stem Cell-Derived Retinal Pigment Epithelium

Claudia Müller,[1] Carol Charniga,[2] Sally Temple,[2] and Silvia C. Finnemann[1,*]
[1]Department of Biological Sciences, Center for Cancer, Genetic Diseases and Gene Regulation, Fordham University, Bronx, NY 10458, USA
[2]Neural Stem Cell Institute, Rensselaer, NY 12144, USA
*Correspondence: finnemann@fordham.edu
https://doi.org/10.1016/j.stemcr.2018.01.017

SUMMARY

With stem cell-derived retinal pigment epithelial (RPE) replacement therapies in clinical testing, establishing potency of RPE prior to transplantation is imperative. Phagocytosis of photoreceptor outer segment fragments (POS) is a key indicator of RPE functionality. Comparing RPE derived from different donor human adult RPE stem cell lines, we found that cells were either high-phagocytic or low-phagocytic despite sharing phagocytic receptors and ligands, junctional ZO-1, and lack of epithelial-mesenchymal transition. We found that low-phagocytic cells harbored F-actin stress fibers but lacked contiguous lateral circumferential F-actin and ezrin-rich microvilli of high-phagocytic cells. Rho kinase inhibition reversed the F-actin phenotype and restored phagocytic capacity to low-phagocytic RPE. Conversely, RhoA activation induced stress fiber formation and reduced phagocytic function of high-phagocytic RPE. These results demonstrate that a stress fiber-rich microfilament cytoskeleton causes phagocytic dysfunction of RPE cells. We propose F-actin assessment as a rapid, sensitive, and quantitative test to identify RPE populations lacking phagocytic capacity.

INTRODUCTION

Retinal pigment epithelial (RPE) replacement strategies for the treatment of retinal degenerative diseases are in development, for example as therapy for age-related macular degeneration, the leading cause of central vision loss of the elderly. Three major stem cell sources are being tested for efficacy following transplantation: differentiated RPE derived from pluripotent human embryonic stem cells (hESCs), from induced pluripotent stem cells (iPSCs), and from adult RPE stem cells (RPESCs). Much effort has been devoted to optimizing the differentiation of differently sourced RPE cells in culture. As recent work has shown, the ability of RPE cells to expand is limited and they have the tendency to undergo culture-related phenotypic changes (Croze et al., 2014; Feng et al., 2010; Singh et al., 2013; Tamiya et al., 2010). After just a few passages, RPE cells in culture may lose their epithelial characteristics and acquire a mesenchymal cell-like phenotype, a process called epithelial-to-mesenchymal transition (EMT) (Grisanti and Guidry, 1995).

Transplanted RPE cells must establish critical functional interactions with photoreceptors in the diseased host retina. Phagocytosis of shed photoreceptor outer segments (POS) is a critical daily task of the RPE *in situ* as outer segment renewal is essential for vision (Mullen and LaVail, 1976; Strauss, 2005; Young, 1967). The continuous process of outer segment renewal involves circadian shedding of distal POS tips that must be completely cleared by the neighboring RPE to maintain retinal homeostasis (LaVail, 1976; Young, 1967; Young and Bok, 1969). RPE cells phagocytose shed POS that have exposed the "eat me" signal phosphatidylserine (PS), while extracellular PS-binding proteins milk fat globule-EGF8 (MFG-E8) and protein S act to bridge POS and receptors on the RPE, αvβ5 integrin, and Mer receptor tyrosine kinase (MerTK), respectively. MFG-E8 and protein S both localize to the subretinal space *in vivo* and are secreted by RPE cells, although additional sources in the retina cannot be excluded (Burgess et al., 2006; Nandrot et al., 2007; Burstyn-Cohen et al., 2012). Complex signaling between αvβ5 integrin and MerTK acting downstream in the cells ultimately accomplish the F-actin cytoskeletal rearrangement that is a prerequisite for POS internalization (Finnemann, 2003; Mao and Finnemann, 2012; Nandrot et al., 2004, 2012).

Rho family guanosine triphosphatases are primary cellular regulators of the F-actin cytoskeleton, with RhoA specifically stabilizing F-actin to promote assembly of contractile actomyosin filaments and stress fibers. In contrast, Rac1 destabilizes F-actin facilitating assembly of branched F-actin networks. Phagocytic mechanisms depend on complex F-actin dynamics (Mao and Finnemann, 2015). During POS phagocytosis, RPE cells must activate Rac1 in an αvβ5 integrin-dependent manner to promote assembly of F-actin beneath surface-tethered POS (Mao and Finnemann, 2012).

Here, we report that an F-actin cytoskeleton rich in stress fibers predicts diminished phagocytic function of differentiated, polarized adult RPESC-derived RPE cells in culture. Moreover, pre-manipulating F-actin of resting RPE to increase or decrease stress fiber abundance is sufficient to decrease or increase their phagocytic activity, respectively. We propose that F-actin cytoskeleton analysis is sufficient to identify RPE cultures with poor phagocytic capacity

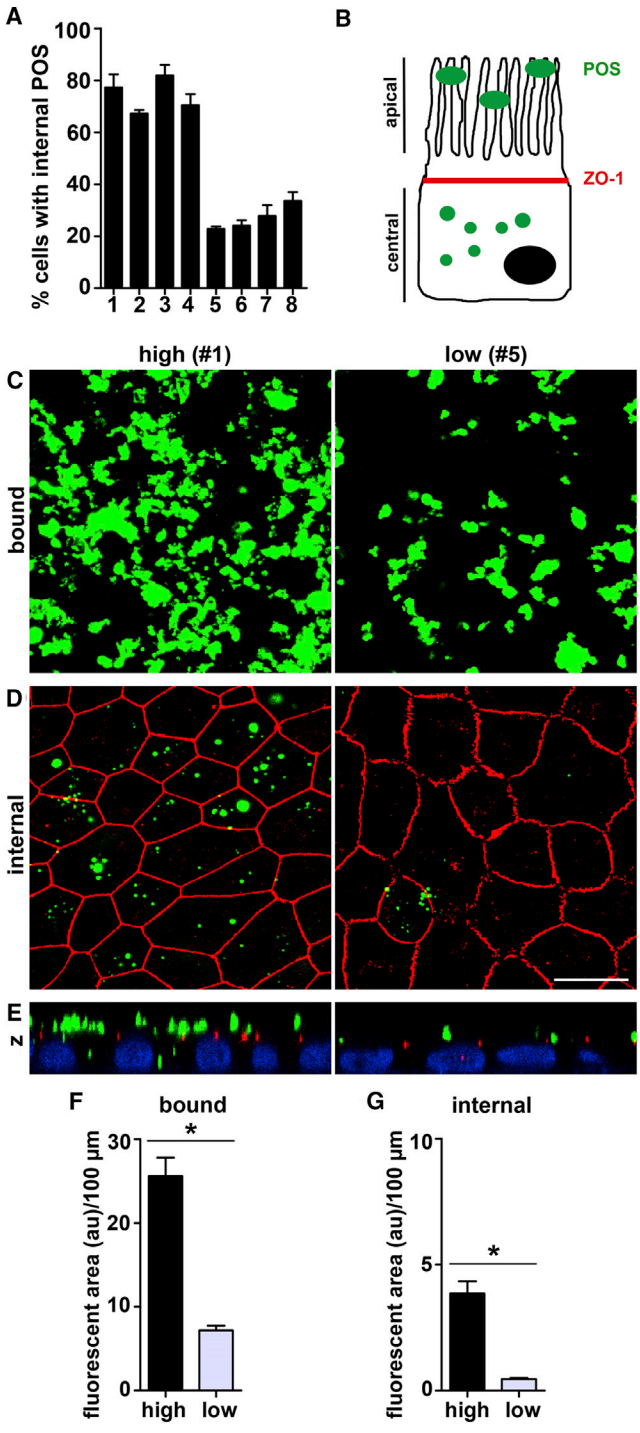

Figure 1. RPE Cell Line Generation Yields Cells that Are Either High or Low Phagocytic

(A) Bars graph shows percentage of cells internalizing POS within 5 hr in a standardized POS phagocytosis assay (see Experimental Procedures) of eight RPE lines each from a different donor generated and grown using identical methodology. Error bars show mean ± SEM, n = 3 independent experiments for each line.

(B) Schematic drawing illustrating the experimental strategy for discrimination of bound and internalized POS.

(C and D) Representative images of high-phagocytic line #1 and low-phagocytic line #5 as indicated show POS (green) that are surface-bound in maximal projections of apical x-y sections (C) or that are internalized in maximal projections of x-y sections representing the central part of the same cells (D). Overlay with ZO-1 staining indicates cell-cell junctional complexes (red). Scale bars, 10 µm.

(E) Representative x-z projections of the experiment shown in (D). Cell nuclei are shown in blue.

(F and G) Bar graphs compare the amount of bound POS material (F) or the amount of internalized POS material (G). Error bars show mean ± SEM, n = 4 different high-phagocytic lines (#1–4) and n = 4 different low-phagocytic lines (#5–8). Asterisks indicate significant difference between high- and low-phagocytic lines by Student's t test. *p < 0.001.

providing a rapid, sensitive, and quantitative quality assessment for RPE cell cultures intended for transplantation. Furthermore, our data indicate that long-term Rho kinase inhibition promotes key RPE functionality by suppressing stress fiber formation.

RESULTS

Human Adult RPESC-Derived RPE Lines Group by Phagocytic Capacity

RPESCs are a small subpopulation of stem cells present in the adult human RPE (Salero et al., 2012). Protocols have been established to expand RPESCs in culture followed by passaging to enrich RPE progeny and differentiation and to yield polarized RPE monolayers that show key characteristics of differentiated RPE cells (Blenkinsop et al., 2013, 2015). Here, we first asked whether human adult RPESC-derived RPE cell populations from different donors generated and grown following the same protocol shared the same phagocytic properties. To this end, eight RPESC-derived RPE lines generated from different donors (Table S1) but using the same protocol and reagents were challenged with purified porcine POS for 5 hr before quantifying bound and internalized POS. Figure 1A shows that RPE cell lines divided into two groups depending on their engulfment activity. Based on confocal microscopy analysis of the fraction of cells binding and internalizing POS (Figure 1B), we categorized lines #1–4 with 67%–82% of cells engulfing POS in our assay as high-phagocytic RPE cells, and lines #5–8 with 23%–34% of cells engulfing POS as low-phagocytic RPE cells.

Representative images from analysis of high-phagocytic RPE line #1 and low-phagocytic RPE line #5 further showed that these cells differed dramatically in both bound and engulfed POS (Figures 1C–1E). Quantification confirmed that

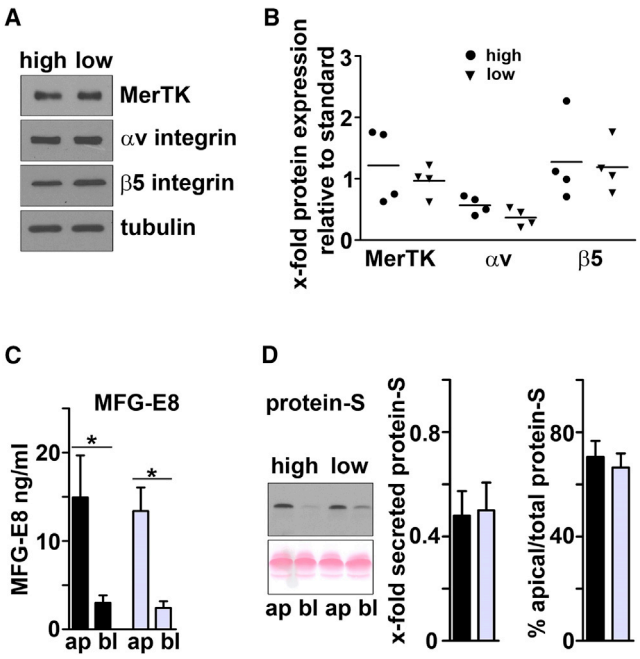

Figure 2. High- and Low-Phagocytic RPE Lines Do Not Differ in Expression of Phagocytic Receptor Proteins αv Integrin, β5 Integrin, or MerTK or in Apical Secretion of Phagocytic Ligands MFG-E8 and Protein S

(A) Representative immunoblot (showing samples from lines #1 and #5) probed sequentially for proteins as indicated.

(B) Quantification of immunoblotting experiments performed as in (A) for all eight RPE lines. Dot plots show relative protein expression as indicated by high-phagocytic lines #1–4 (circles) and low-phagocytic lines #5–8 (triangles). Each protein was quantified compared with tubulin as a loading control and relative to a standard included on all gels, and consisting of a mixed-cell line sample; symbols indicate mean of n = 3 independent samples for each line. Student's t test did not show significant differences between the averages of high- and low-phagocytic RPE cells.

(C) Absolute levels of secreted MFG-E8 in ng/mL measured by ELISA in supernatants collected from the apical (ap) and basal (bl) chambers of transwell inserts of RPE cells as indicated. Supernatants were collected 72 hr after complete medium change. Error bars show mean ± SEM, n = 4 high-phagocytic lines (black bars, *p < 0.05) and 4 low-phagocytic lines (gray bars, *p < 0.01). Asterisks indicate significant difference of apical and basal MFG-E8 content as indicated by Student's t test.

(D) Representative protein S immunoblot supernatants retrieved from apical and basal chambers of high-phagocytic RPE line #1 and low-phagocytic RPE line #5, as indicated, after 4 weeks of culture. Non-specific protein stain of the membrane before block is shown to demonstrate similar load. Left bar graph shows relative total (apical plus basal) secreted protein S levels of the 4 high-phagocytic lines (black bars) and the 4 low-phagocytic lines (gray bars) quantified compared with a standard of purified human protein S (Hyphen Biomed) included on all gels, mean ± SEM. Right bar graph shows percentage of apical protein S of total protein S, mean ± SEM, n = 4 high-phagocytic lines (black bars) and 4 low-phagocytic lines (gray bars). Differences were not significant.

the low-phagocytic line #5 had 76% less POS material bound to the cell surface and 89% less POS material internalized than the high-phagocytic line #1. Quantification of images from experiments testing all eight RPE lines revealed that the four low-phagocytic lines on average bound 72% less POS material and internalized 88% less material than high-phagocytic cells (Figures 1F and 1G). Altogether, low-phagocytic RPE lines were significantly impaired in phagocytic function compared with high-phagocytic RPE lines with respect to the fraction of phagocytic cells as well as the capacity of cells to bind and engulf POS.

Low- and High-Phagocytic RPE Cells Do Not Differ in Expression of Phagocytic Receptors αvβ5 Integrin and MerTK or Secretion of Phagocytic Ligands MFG-E8 and Protein S

We then tested whether low-phagocytic cells lacked key components of the machinery used by RPE cells to phagocytose POS. We thus determined protein expression levels of the subunits of the POS binding receptor αvβ5 integrin and the POS engulfment receptor MerTK. Immunoblotting detected receptor proteins in all eight cell lines tested. Levels of receptor proteins varied somewhat among cell lines, but there was no significant difference between high- and low-phagocytic RPE cells (Figures 2A and 2B).

In vitro cell culture POS phagocytosis assays require supplementation of extracellular bridge ligand proteins MFG-E8 and protein S because repeated supernatant media change during the procedure removes endogenous ligands secreted by RPE (Mayerson and Hall, 1986; Nandrot et al., 2007). Thus, differences in RPE phagocytic activity measured in our POS challenge assays do not reflect differences in secretion of MFG-E8 or protein S. However, to determine to which extent our RPE cell lines secrete these important ligand proteins, we next quantified endogenous phagocytic ligands in media collected from the apical and basolateral side of RPE cultures after prolonged incubation. By ELISA and western blotting we found polarized apical secretion of MFG-E8 and protein S, the physiological retinal ligands of αvβ5 integrin and MerTK, respectively (Figures 2C and 2D). We detected similar levels of MFG-E8 in apical supernatant medium of high- and low-phagocytic cells, which was exposed to the cultures for 72 hr (Figure 2C). In the same supernatant medium we failed to detect protein S secretion by immunoblotting in either cell line. However, protein S was detected in supernatant medium retrieved from 4-week-old cultures where it was found at similar levels and mainly apically in high- and low-phagocytic lines (Figure 2D).

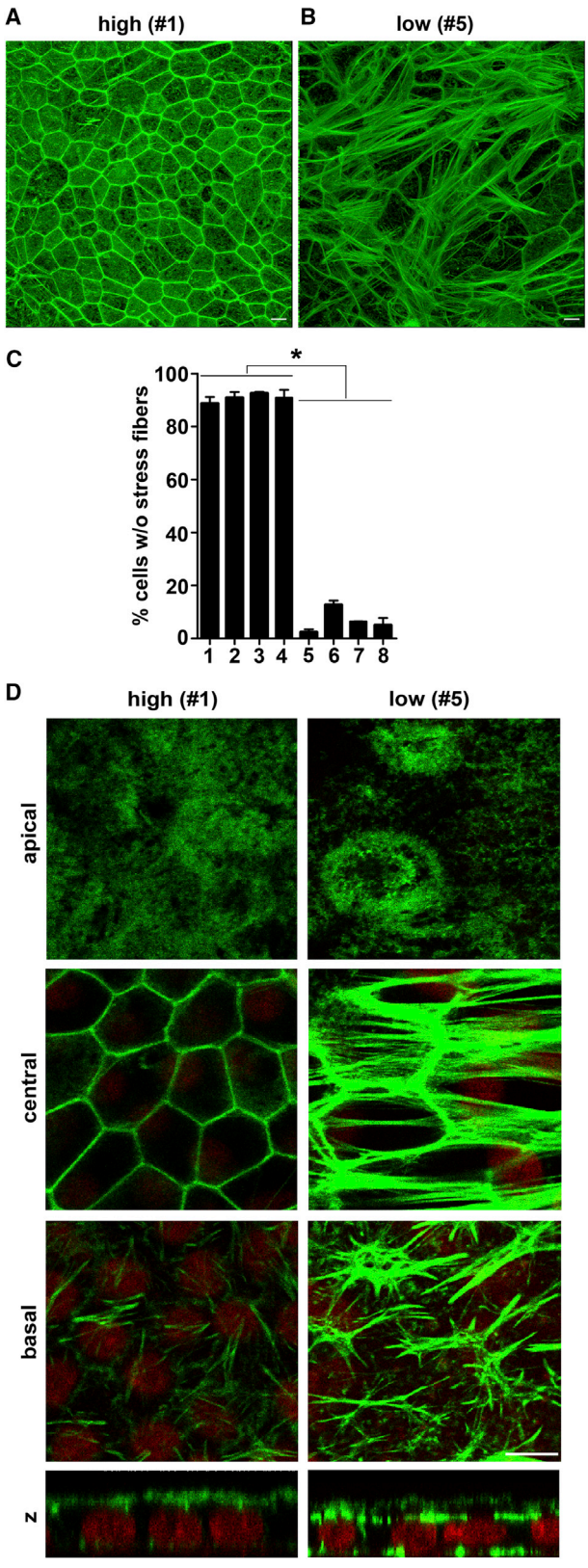

Figure 3. Low-Phagocytic RPE Cells Possess a Highly Abnormal F-Actin Cytoskeleton Characterized by Lack of Lateral Circumferential F-Actin, Less Apical F-Actin, and Abundant Stress Fibers

(A and B) Images show acquired representative maximal projections of F-actin (green) for high-phagocytic RPE line #1 (A) or low-phagocytic RPE line #5 (B) as indicated using identical imaging settings.

(C) Bar graph shows percentage of cells with complete lateral circumferential F-actin and no stress fibers in each of the eight RPE lines as indicated. Error bars show mean ± SEM, n = 3 independent experiments for each line. Asterisks indicate significant differences between cell lines as indicated by lines by one-way ANOVA. *$p < 0.0001$.

(D) Representative images obtained using identical imaging settings show F-actin (green) and cell nuclei (red) co-stains in separate individual x-y confocal sections representative for apical, central, and basal aspects of cells and an x-z section of the same field of high- and low-phagocytic RPE cell lines #1 and #5 as indicated.

Scale bars, 10 μm.

RPE Cells with Low-Phagocytic Capacity Show an Abnormal Epithelial F-Actin Cytoskeleton without Complete Lateral Circumferential F-Actin but Containing Abundant Stress Fibers

A dynamic F-actin cytoskeleton that can be mobilized and recruited beneath bound particles is a prerequisite for POS clearance phagocytosis (Mao and Finnemann, 2015). To assess F-actin morphology, we examined the F-actin cytoskeleton by confocal microscopy in all eight cell lines. Observing total cellular F-actin at low magnification, we found a striking difference between high- and low-phagocytic lines #1 and #5 (Figures 3A and 3B). In high-phagocytic RPE line #1, fields without exception showed a highly regular distribution of cells with contiguous lateral circumferential F-actin. In contrast, in low-phagocytic RPE line #5, most fields showed cells with diverse F-actin arrangement including prominent stress fibers. The fields shown are representative for all eight RPE lines. Specifically, high-phagocytic RPE lines contained 89%–93% cells without stress fibers, while this fraction fell to 3%–13% in low-phagocytic lines (Figure 3C). Further assessing F-actin structures in specific subcellular regions at high magnification, we found that most high-phagocytic cells had an F-actin-rich apical brush border, clearly defined contiguous circumferential lateral F-actin that outlined the hexagonal shape of the cells, and a moderate number of basal focal adhesions (Figure 3D, high, #1). In contrast, low-phagocytic lines were composed mainly of cells with varied shape of reduced height that contain less apical F-actin, but abundant central F-actin stress fibers and a high number of basal focal adhesions (Figure 3D, low, #5). The robust signals from central stress fibers and basal infoldings lead to an

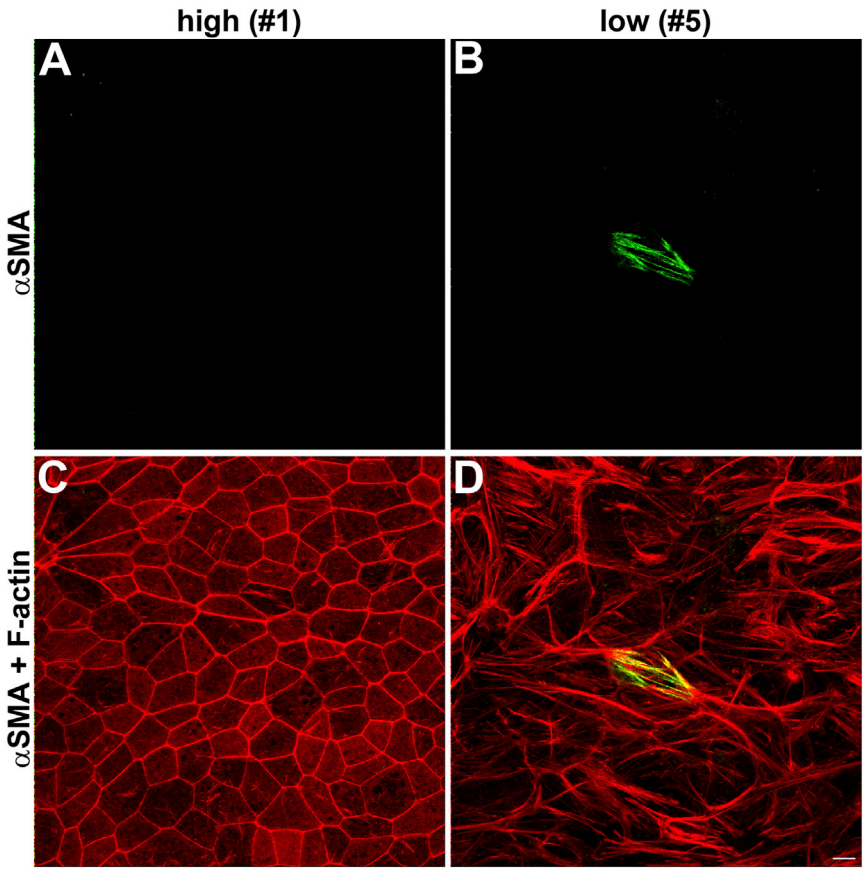

Figure 4. Only a Small Percentage of High- and Low-Phagocytic RPE Cells Express the Mesenchymal Marker Protein α-Smooth Muscle Actin

Representative x-y maximal projections of high-phagocytic RPE line #1 (A and C) and low-phagocytic RPE line #5 (B and D) show staining of smooth muscle actin (αSMA, green) alone (A and B) or merged with F-actin (red) (C and D). Similar results were obtained for all eight RPE lines (see Results). Scale bar, 10 μm.

overall brighter appearance of central and basal F-actin in low-phagocytic cells. Altogether, these experiments reveal a dramatic difference in F-actin cytoskeleton between high- and low-phagocytic RPE cells, with stress fiber formation directly correlating with low phagocytic activity.

Low-Phagocytic Cells with Abnormal F-Actin Do Not Express α-Smooth Muscle Actin that Indicates Epithelial-Mesenchymal Transition

Expansion of RPE cells in culture may trigger RPE cell dedifferentiation and EMT (Grisanti and Guidry, 1995). The studied cells of the low-phagocytic line had moderately lower cell density and height per cell (Figure 3D). To determine whether low-phagocytic cells lacked epithelial differentiation, we tested the expression of α-smooth muscle actin (αSMA), a widely used marker of EMT. Figure 4 shows that most high- or low-phagocytic cells did not express αSMA under the experimental conditions used. We deliberately show a field in which one cell is labeled by αSMA antibody, which serves as positive control for our antibody staining. Image quantification revealed that our four low-phagocytic RPE lines contained 1.0%–2.7% αSMA-positive cells, while in the same lines and under the same culture conditions 87%–97% of the cells showed abnormal F-actin. This experiment confirmed that low-phagocytic function and abnormal F-actin cytoskeleton in our RPE lines are not due to EMT.

Diminished Expression of RPE Marker Proteins Correlates with Abnormal F-Actin Organization in Low-Phagocytic Cells

We next assessed the extent to which high- and low-phagocytic lines maintained known RPE characteristics. Compared with high-phagocytic RPE cells, we found significantly lower abundance and extension of ezrin-rich microvilli at the apical surface and reduced ezrin expression levels of low-phagocytic RPE cells (Figures 5A [top row] and 5B–5D). The level of the cytoplasmic visual cycle enzyme RPE65 was also lower in low-phagocytic than in high-phagocytic cells (Figures 5A [center row] and 5B–5D). Notably, low-phagocytic cells possessed lateral ZO-1 tight junction associated protein at lateral borders like high-phagocytic cells (Figures 5A [bottom row] and 5B). We noticed a somewhat distinct appearance of ZO-1 in high-phagocytic cells with signals of uniform intensity marking straight cell borders, while the ZO-1 signal in low-phagocytic cells often showed interruptions and the borders were wavy (Figure 5A, bottom row). However,

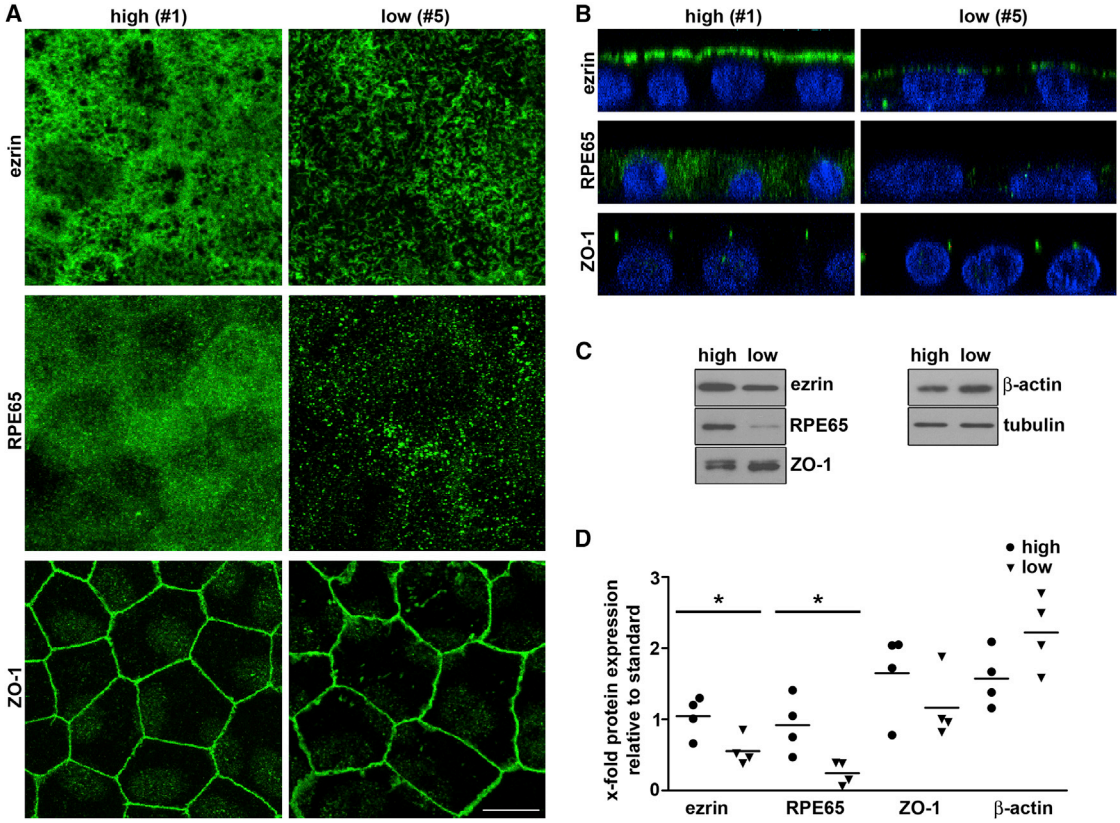

Figure 5. Low-Phagocytic RPE Cells Show Moderate Differences in the Visual Cycle Enzyme RPE65 and Ezrin, an Essential Constituent of RPE Microvilli

(A) Representative x-y maximal projections show ezrin, RPE65, and ZO-1 (all green) in high-phagocytic RPE line #1 and low-phagocytic RPE line #5 as indicated. Scale bar, 10 μm.

(B) X-z projections of the same fields as in (A) are shown with green protein stains as indicated, and as in (A) merged with nuclei (blue) labels.

(C) Representative immunoblot membrane of lysates from high-phagocytic RPE line #1 and low-phagocytic RPE line #5 probed sequentially for proteins as indicated.

(D) Dot plots show quantification of proteins in all four high-phagocytic lines (circles) and all four low-phagocytic lines (triangles) as indicated. Each protein was quantified compared with tubulin loading control and relative to a standard included on all gels and consisting of a mixed-cell line sample; symbols show mean of n = 3 independent samples for each line. Asterisks and lines indicate significant difference between the averages of high- and low-phagocytic RPE cell lines by Student's t test. *$p < 0.05$.

while levels of ZO-1 protein were variable between lines there was no significant difference specifically between low- and high-phagocytic lines (Figures 5C and 5D). The same was true for β-actin (Figures 5C and 5D).

ROCK Inhibitor Restores Both Epithelial F-Actin Organization and High-Phagocytic Capacity to Low-Phagocytic RPE Cells, while Rho Activator Renders High-Phagocytic RPE Less Phagocytic

We postulated that stress fiber formation in low-phagocytic RPE cells involved elevated RhoA activity. We therefore tested the effects of manipulation of RhoA signaling by RhoA activating compound or by inhibition of RhoA downstream mediator Rho kinase (ROCK) on F-actin organization and phagocytic activity of low- and high-phagocytic RPE cells. Initial experiments inhibiting RhoA signaling with ROCK inhibitor for up to 24 hr did not obviously alter F-actin morphology of low-phagocytic RPE cells (data not shown). However, treatment with ROCK inhibitor for 7 days was without obvious effect on high-phagocytic RPE cell line #1 (compare Figures 6A and 6D) but greatly increased the fraction of low-phagocytic RPE cells in line #5 with contiguous lateral circumferential F-actin and without stress fibers from 1% to 90%, with large fields of cells with uniform epithelial appearance (compare Figures 6B and 6E). The same treatment followed by quantification of F-actin structures of six RPE lines revealed that ROCK inhibitor had no effect on average F-actin

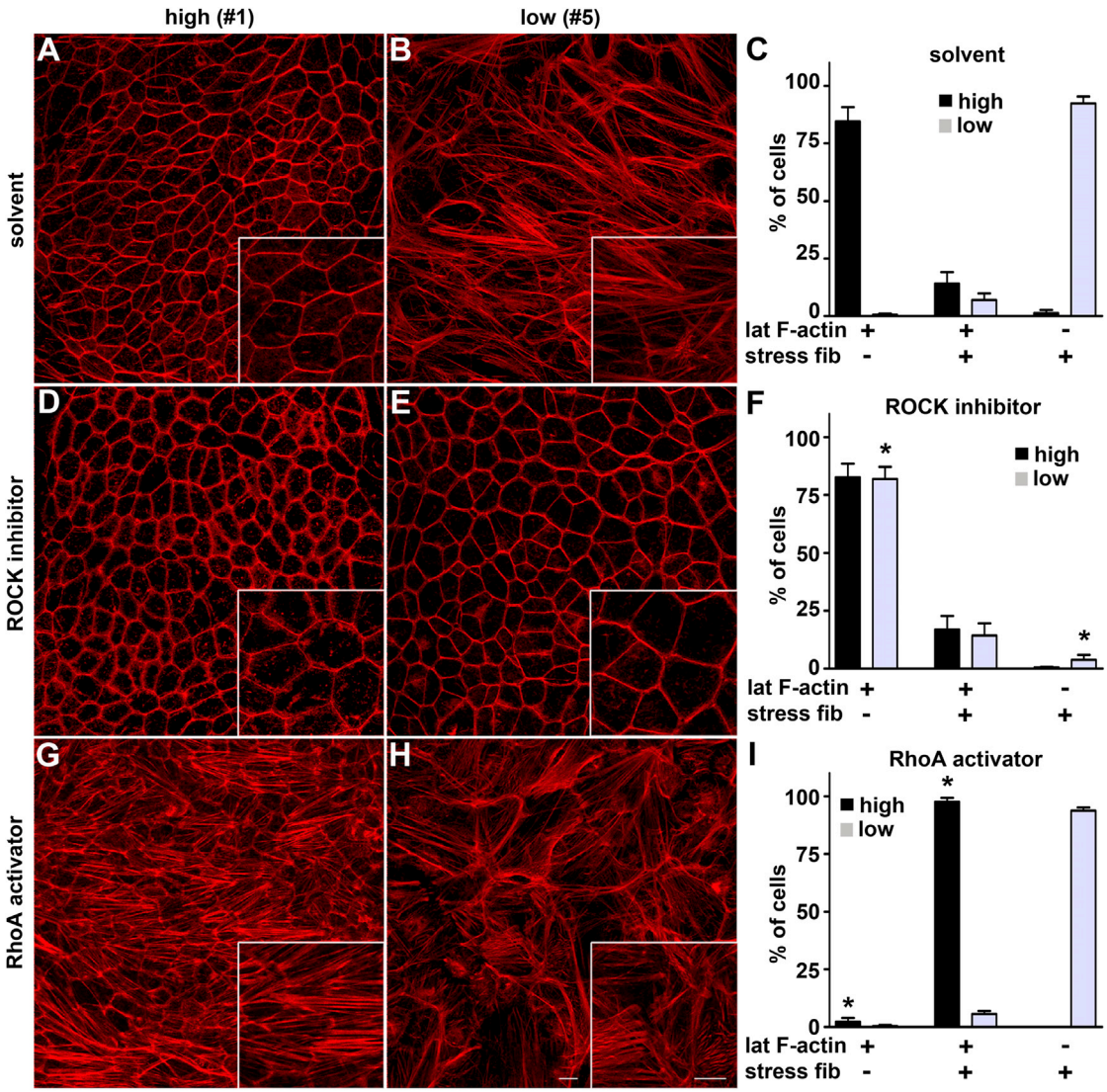

Figure 6. Manipulation of RhoA/ROCK Signaling Is Sufficient to Switch F-Actin Phenotype between High- and Low-Phagocytic RPE Cells

(A, B, D, E, G, and H) Representative x-y maximal projections show F-actin labeling of high- or low-phagocytic RPE cells (line #1 and #5, respectively) as indicated after treatment for 7 days with solvent (A and B), ROCK inhibitor (D and E), or RhoA activator (G and H). Scale bars, 10 μm.

(C, F, and I) Bar graphs show percentage of cells with lateral circumferential F-actin, stress fibers, or both after treatment with solvent, ROCK inhibitor, or RhoA activator as mean ± SEM, n = 3 lines each of high- and low-phagocytic RPE (black bars, high-phagocytic lines #1–3; gray bars, low-phagocytic lines #5–7). Asterisks indicate a significant change in fraction of cells with specific F-actin phenotype with drug treatment as indicated compared with solvent treatment in either high- or low-phagocytic RPE lines as established by one-way ANOVA. *$p < 0.001$.

distribution of cells in high-phagocytic RPE lines (compare black bars in Figures 6C and 6F) yet dramatically increased the average fraction of cells in low-phagocytic RPE lines with circumferential lateral F-actin and without stress fibers (compare gray bars in Figures 6C and 6F). Indeed, F-actin scores were similar of high- and low-phagocytic RPE lines after ROCK inhibitor treatment (Figure 6F, compare black and gray bars). Conversely, pre-treatment with RhoA activator caused formation of stress fibers in 96% of high-phagocytic cells of line #1 but, notably, these cells retained circumferential F-actin (compare Figures 6A and 6G). Similar results were obtained for all high-phagocytic lines tested (black bars in Figures 6C and 6I). RhoA activator had negligible effects on F-actin in low-phagocytic cells

(compare Figures 6B and 6H, and compare gray bars in Figures 6C and 6I). Neither drug treatment caused visible cytotoxicity or significantly altered the transepithelial resistance of cultures.

Finally, we asked whether RhoA/ROCK pathway modulation as shown for Figure 6 was sufficient to alter RPE phagocytic function. RhoA activator pre-treatment of high-phagocytic cells reduced their capacity to bind and internalize POS on average 2.4-fold and 5.8-fold, respectively, compared with the same cells treated with solvent (Figure 7A as indicated; black bars Figures 7C and 7D), and to the level of low-phagocytic cells, whose phagocytic activity was not affected by RhoA activator (gray bars in Figures 7C and 7D). Strikingly, ROCK inhibitor pre-treatment was sufficient to significantly increase POS binding as well as POS internalization by low-phagocytic RPE cells on average 2.9-fold and 3.8-fold, respectively, over the same cells treated with solvent (Figure 7B as indicated; gray bars Figures 7C and 7D). ROCK inhibitor did not alter POS binding by high-phagocytic RPE cells, and a modest increase in POS internalization did not reach statistical significance (Figures 7C and 7D, black bars). Taken together, RhoA activation impaired morphology and phagocytic function of high-phagocytic RPE cells. ROCK inhibition was sufficient to restore both epithelial F-actin morphology and phagocytic function to low-phagocytic RPE cells.

DISCUSSION

RPE cells differentiated from different source stem cell types are under development for clinical application worldwide. Comprehensive quality criteria for such engineered cells are needed to ensure consistency of cell products. Cellular assay data exchange and reproducibility among laboratories are limited to date due to lack of standardized testing methodology and well-defined quantitative quality criteria. In this study we present donor-based heterogeneity in epithelial F-actin cytoskeleton organization in different adult RPESC-RPE lines and demonstrate a causal relationship of an F-actin cytoskeleton rich in stress fibers with the capacity of RPE lines to phagocytose POS *in vitro*. We propose F-actin phenotype scoring as a rapid, sensitive, and quantitative assessment method to be included in RPE cell quality assessment and reporting.

POS phagocytosis is a key and characteristic function of RPE cells that is essential for photoreceptor support. It is therefore accepted as a required functionality trait and a key quality indicator of model RPE cells in culture. Unfortunately, RPE cell culture phagocytosis assays are multistep experiments for which no accepted standards exist (e.g., with respect to phagocytosis receptor ligand supplementation or incubation times) and which involve numerous laboratory-made reagents such as mechanically isolated outer segment preparations. RPE phagocytosis studies feeding synthetic particles do not necessarily yield insight into the machinery and activities of RPE that are relevant to their POS uptake (Heth and Marescalchi, 1994). RPE cells of the MerTK-deficient RCS (Royal College of Surgeons) rat lack the ability to internalize POS but are able to engulf latex beads, indicating that these particles are taken up by different cellular machinery (Edwards and Szamier, 1977). Moreover, numerous experimental approaches are being used to quantify POS phagocytosis, with some, but not all, distinguishing between POS binding and engulfment.

Here, we use confocal microscopy to distinguish bound and internalized POS in the same intact fixed RPE monolayers based on their location relative to the tight junction marker ZO-1. This approach does not require cell manipulation for removal (e.g., using EDTA-containing buffer) or fluorescence quenching of surface-bound POS (e.g., using trypan blue solution), which have been used to exclude bound POS from quantification (Finnemann et al., 1997; Mao and Finnemann, 2012, 2013). We found that highly polarized RPESC-RPE cells have the capacity to bind large numbers of intact POS, whose complete removal or quenching risks damaging cells and possibly leading to inconclusive results. Taken together, as a result of discrepancies in assay execution and uptake measurements, data obtained from RPE phagocytosis assays performed in different laboratories are not directly comparable.

Our results show that an F-actin cytoskeleton rich in stress fibers directly predicts poor phagocytic activity and that lack of stress fibers in conjunction with contiguous lateral circumferential F-actin directly correlates with high-phagocytic activity of RPESC-RPE cells. It should be noted here that RPE cells possess key characteristics other than phagocytic activity that we did not test, and that may or may not correlate with the F-actin phenotype. For instance, functions of RPE cells in culture may change with passaging despite overall similar appearance (Pilgrim et al., 2017). In our high-phagocytic lines, the vast majority of cells possessed lateral circumferential F-actin while also lacking stress fibers. In these cells induction of stress fibers by Rho activator was sufficient to stimulate stress fibers and dramatically reduce phagocytic activity, although these cells maintained circumferential lateral F-actin. Thus, the presence of stress fibers alone is sufficient to directly predict low-phagocytic activity of RPE cells. In contrast to phagocytosis assays, F-actin labeling with phalloidin is a rapid one-step staining method using only commercially available reagents. F-actin stress fibers and epithelial lateral circumferential F-actin are robust in appearance, facilitating imaging and image quantification. We predict that

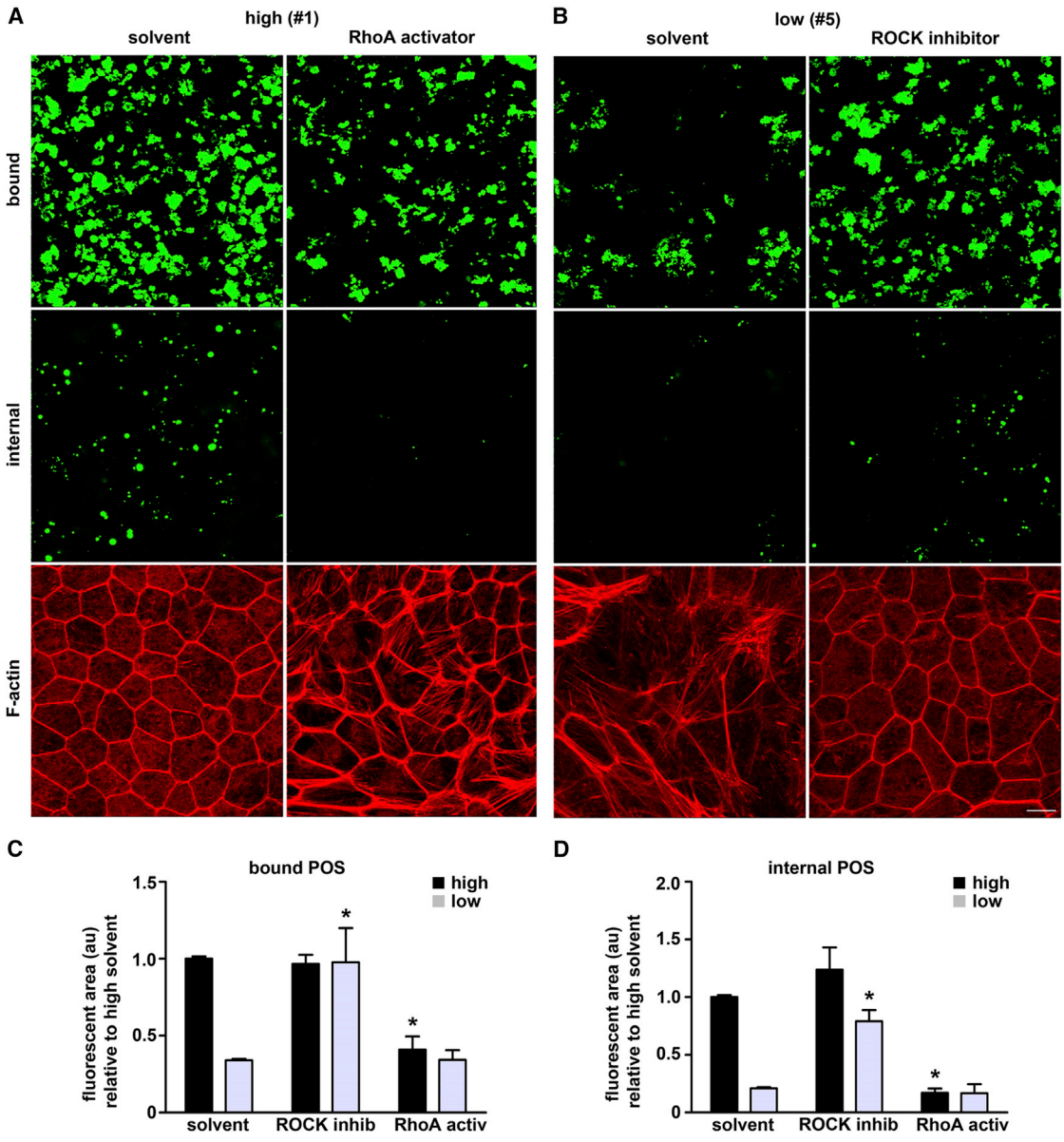

Figure 7. Manipulation of RhoA/ROCK Signaling Is Sufficient to Switch Phagocytic Capacity between High- and Low-Phagocytic RPE Cells

(A) Representative images obtained of high-phagocytic RPE cells (line #1) treated for 7 days with solvent or RhoA activator as indicated show bound POS (top row, apical projections, green), internal POS (center row, central projections, green), or F-actin (bottom row, total maximal projections, red).

(B) Representative images obtained of low-phagocytic RPE cells (line #5) treated for 7 days with solvent or ROCK inhibitor as indicated show bound POS, internal POS, and F-actin as described for (A). Scale bar, 10 μm.

(C and D) Bar graphs show quantification of bound (C) and internalized (D) POS in 100-μm^2 fields of experiments as in (A) and (B); mean ± SEM, n = 3 lines each of high- and low-phagocytic RPE (black bars, high-phagocytic lines #1–3; gray bars, low-phagocytic lines #5–7). Asterisks indicate a significant difference of bound or internal POS with drug treatment as indicated compared with solvent treatment in either high- or low-phagocytic lines as established by one-way ANOVA. (C) black bars, *$p < 0.01$; gray bars, *$p < 0.05$. (D) black bars, *$p < 0.01$; gray bars, *$p < 0.01$.

including quantifying F-actin organization as described in our study and specifically scoring the fraction of RPE with stress fibers will yield results that are highly consistent among laboratories, an important advance.

Our results suggest significant variance in the phagocytic capacity of cultured RPE cells. Variability between cultures may arise due to inconsistent cell preparation and maintenance, or intrinsic genetic and epigenetic differences between different donors or starting tissues. A recently reported study extensively evaluating RPE-specific phenotype and function of 15 iPSC-RPE lines and revealed that donor-to-donor variability of iPSC-RPE functions exceeded clone-related variation resulting from epigenetic differences due to different starting tissues (Miyagishima et al., 2016). We cannot exclude that technical issues contribute to the cell line differences we found, despite our best efforts in isolating and maintaining each RPESC-RPE line under identical conditions. However, RPE lines grouped into either high- or low-phagocytic with low-phagocytic lines convertible to high-phagocytic by 7 days of ROCK inhibition suggest donor intrinsic rather than experimentally induced variability. A recently reported study extensively evaluating RPE-specific phenotype and function of 15 iPSC-RPE lines compared with primary human fetal RPE in culture revealed donor- or clone-related variation in iPSC-RPE function resulting from epigenetic differences due to different starting tissues (Miyagishima et al., 2016). Another study demonstrated that variations in hepatic differentiation of iPSC are largely due to differences between donors (Kokkinaki et al., 2011).

Expression of phagocytic ligands MFG-E8 and protein S was previously demonstrated using rodent tissues and RPE in culture (Burgess et al., 2006; Nandrot et al., 2007). Here we show that human RPESC-RPE cells secrete both MFG-E8 and protein S. Steady-state expression levels of phagocytic receptors were similar in RPE lines regardless of whether they were high- or low-phagocytic. In contrast, Westenskow et al. (2012) showed that αvβ5 integrin expression predicted the rate of POS phagocytosis of their human ESC- or iPSC- derived RPE cells in culture. In our study, neither the amount of opsonizing bridge molecules secreted nor the levels of phagocytic receptor proteins correlated with phagocytic capacity of RPESC-RPE cells.

Like high-phagocytic RPE cells, low-phagocytic RPE cells lacked the mesenchymal marker protein αSMA and retained localization of the tight junction associated protein ZO-1 at cell-cell contacts. These results suggest that low-phagocytic RPE cells redifferentiated into an epithelial phenotype during the post-proliferative phase in culture (Choudhary et al., 2016). Furthermore, they imply that scoring F-actin organization as described provides information of RPE-like characteristics beyond testing epithelialization.

Presence of stress fibers may reduce POS phagocytosis by reducing F-actin availability for structures needed for phagocytosis. Decreased apical ezrin expression and reduced apical F-actin likely in apical processes in low-phagocytic cells implies shorter and fewer apical surface microvilli that may allow less POS binding and, in consequence, less POS internalization. Moreover, POS internalization may be affected by lack of direct F-actin availability (Mao and Finnemann, 2015). Engulfment requires formation of the so-called phagocytic cup beneath bound particles, a transient assembly of crosslinked F-actin that facilitates extension of membrane protrusions around the bound particle. Ach et al. (2015) recently reported F-actin stress fibers in well-preserved human eyes with age-related macular degeneration. This study, in agreement with ours, implies that stress fibers in RPE cells are abnormal and should be avoided in replacement cells and culture experiments aiming to study physiologically normal RPE (while acknowledging that even RPE in culture without stress fibers likely differs in F-actin morphology from RPE in the intact retina *in situ*). Reduced phagocytosis due to extensive intracellular polymerization of F-actin and stress fiber formation in insect hemocytes by *Photorhabdus luminescens* toxin may be another similar scenario that is relevant in nature (Lang et al., 2010).

ROCK inhibitor Y-27632 has been added to RPE cultures in studies aiming to generate RPE for transplantation purposes, as it is known to improve RPE differentiation and to allow repeat passaging (Croze et al., 2014). ROCK inhibitor is thought to promote RPE proliferation by inducing cell cycle progression and by inhibition of key ligands of transforming growth factor β and Wnt signaling pathways, thus suppressing EMT (Buchholz et al., 2013; Croze et al., 2014). Here, we expand on this observation by demonstrating the effect of this treatment on F-actin and its sufficiency to revert low- to high-phagocytic RPE cells. Notably, ROCK inhibitor treatment required several days before F-actin reorganization was apparent and low-phagocytic cells regained their phagocytic capacity. As treatment was performed on post-confluent RPE monolayers, effects studied here were largely independent of cell proliferation. Lack of adverse effect of ROCK inhibitor on high-phagocytic RPE cells suggests that ROCK inhibitor may be added routinely to RPE cell cultures.

EXPERIMENTAL PROCEDURES

All materials were from Thermo Fisher or Corning unless otherwise indicated.

Human RPE Cell Culture

Procedures were reviewed and deemed exempt by the IRBs of Fordham University and Albany Medical College. Human RPESCs were

isolated from eyes donated to registered eye banks following a protocol adapted from Blenkinsop et al. (2013). This procedure expands a population of adult RPESCs followed by differentiation into polarized RPE monolayers. RPESC-derived RPE phenotype, functional characteristics, and utility in transplantation have been described previously (Blenkinsop et al., 2015; Davis et al., 2017). Donor, tissue procurement, and cell yield information for the eight RPE lines used in this study is provided in Table S1. In brief, globes were enucleated and immediately wrapped in saline-moistened sterile gauze, placed into separate small chambers, and inserted into a stabilizing foam holder followed by overnight priority shipping. Globes were cut circumferentially below the ora serrata to remove the cornea, followed by removal of vitreous and neural retina. Eyecups were rinsed with PBS (without Ca^{2+} and Mg^{2+}) before incubation in 0.25% trypsin and 0.913 mM EDTA in saline (Thermo Fisher) supplemented with 12 μg/mL DNase (STEMCELL Technologies) for 30 min in a humidified incubator at 37°C and 5% CO_2. The RPE were gently brushed off the underlying Bruch's membrane and collected in a tube with RPE differentiation medium (50% DMEM/F12, 50% MEM-α medium, 10 mM niacinamide [Spectrum Chemical], penicillin/streptomycin, sodium pyruvate, non-essential amino acids [all 1:100], L-glutamine, N1 supplement [both 1:200], 500 mg/L taurine, 40 μg/L hydrocortisone, and 26 ng/L triiodothyronine [all MilliporeSigma]) supplemented with 10% heat-inactivated fetal bovine serum (FBS), pelleted at 259 × *g* for 5 min, and seeded in the same medium on Synthemax-coated 24-well culture plates (SynthemaxII-SC at 25 μg/mL) at 100,000 cells per well. Cells were maintained in a 37°C, 5% CO_2 humidified incubator in RPE differentiation medium supplemented with 10% FBS for 3 days before changing to RPE differentiation medium supplemented with 2% FBS. Fifty percent of the medium was replaced weekly on days 1 and 5, with a simple addition of 25% of the volume of medium on day 3. After growing cells for 7–8 weeks, cells were reseeded in Synthemax-coated 24-well plates at 100,000 cells per well. These passage-1 cells were cryopreserved after 7 weeks and then thawed as needed, and plated as passage 2 at 20,000 cells per 6.5-mm Synthemax-coated transwell filter (Corning #3470). Passage-2 cells were used for all experiments 4–5 weeks after seeding. Transepithelial electrical resistance (TER) values of all eight RPE lines were similar, ranging from 142 to 165 Ω cm^2. The average TER of the four high-phagocytic lines was 155 ± 10 Ω cm^2 and of the four low-phagocytic lines 151 ± 5.9 Ω cm^2; this difference was not significant according to Student's t test (mean ± SEM; n = 4 lines with four independent samples measured per line; p = 0.60). These TER averages are slightly below the average TER reported previously for RPESC-RPE after 8 weeks of culture in agreement with a continued rise in TER of RPESC-RPE post confluence (Blenkinsop et al., 2015). For select experiments, cells 3 weeks after plating were treated for 7 days with 10 μM Rho kinase (ROCK) inhibitor Y-27632, or 0.1 μg/mL Rho Activator II (both from Cytoskeleton) or an equal volume of water as solvent control. Additives were applied with each change of culture medium.

Phagocytosis Assay

POS fragments were purified from fresh porcine eyes and covalently labeled with fluorescein isothiocyanate directly before use following published protocols (Parinot et al., 2014), Prior to POS challenge, RPE cells received DMEM supplemented with 10% FBS for 2 hr, followed by a 45-min incubation and two rinses with serum-free DMEM. As these medium changes remove endogenous ligands and to ensure equal availability of soluble ligand proteins across samples, RPE cells were then challenged with 10 POS/cell in serum-free DMEM supplemented with 2.5 μg/mL human MFG-E8 (Biotechne) and 2 μg/mL protein S (Hyphen Biomed). After 5 hr, RPE cells were washed four times with PBSCM (PBS supplemented with $CaCl_2$ and $MgCl_2$) before methanol fixation and immunostaining with ZO-1 antibody and AlexaFluor 594 conjugated secondary antibodies. Stacks of x-y images were acquired with a Leica TSP5 laser scanning confocal microscopy system (Leica Microsystems, Wetzlar, Germany). ImageJ software and Adobe Photoshop CS5 were used to compile and analyze images. X-y image z stacks displaying the entire cell were separated into two non-overlapping apical and central z stacks: the apical z stack was selected to show only bound POS located above the tight junction signal and the central z stack was selected to show only internalized POS below the tight junctions. Projections of apical and central z stacks allowed us to separately display and quantify bound and internalized POS.

Immunofluorescence Microscopy

For F-actin cytoskeleton and RPE marker protein labeling, cells were fixed with 4% paraformaldehyde in PBSCM for 10 min followed by 10 min incubation in PBS with 1% BSA and 0.5% Triton X-100 at room temperature. For F-actin labeling, cells were incubated overnight with AlexaFluor488-conjugated phalloidin at 1:50 in PBS with 1% BSA. For evaluation of marker protein expression, cells were incubated with primary antibodies to antigens as follows: RPE65 (GTX103472, Genetex), smooth muscle actin (ab7817, Abcam), ezrin (sc20773, Santa Cruz Biotechnology), and GAPDH (6C5, Biotechne). AlexaFluor-conjugated secondary antibodies and DAPI nuclei stain were used. Horizontal (x-y) and vertical (z) images were acquired using Leica TSP5 laser scanning confocal microscopy system. Acquired images showing nuclei and F-actin double labeling were analyzed by a human observer with automated bookkeeping using ImageJ software. Adobe Photoshop CS5 was used to compile and analyze images.

Western Blot Analysis

For analysis of whole-cell lysates, cells were solubilized with HNTG buffer (50 mM HEPES [pH 7.4], 150 mM NaCl, 1.5 mM $MgCl_2$, 10% glycerol, 1% Triton X-100) supplemented with 1 mM PMSF and 1% protease inhibitor cocktail (MilliporeSigma) by shaking for 30 min at 4°C. Cell lysates representing equal cell numbers were compared by immunoblotting. For evaluation of secretion of protein S cell culture, supernatants from 4-week-old cultures were analyzed by immunoblotting using standard protocols followed by chemiluminescence detection (PerkinElmer). Antibodies used for immunoblotting were as listed for immunofluorescence and β-actin antibody (A2066, MilliporeSigma). ImageJ was used for densitometry of scanned X-ray films.

ELISA

Supernatant media were collected from the apical and basal chambers 72 hr after medium change. The amount of MFG-E8 protein

was determined by ELISA according to the manufacturer's instructions (Biotechne).

Statistical Analysis

All experiments were performed comparing 6–8 RPE lines (3–4 high- and 3–4 low-phagocytic) each derived from a different donor (Table S1). Prism was used for statistical analysis. Student's t test was used to compare between two samples. For more than two samples, we used Welch's ANOVA test (one-way ANOVA with unequal variances) followed by Tukey-Kramer post hoc test to compare specific samples. $p < 0.05$ was chosen as threshold for statistically significant difference between samples.

SUPPLEMENTAL INFORMATION

Supplemental Information includes one table and can be found with this article online at https://doi.org/10.1016/j.stemcr.2018.01.017.

AUTHOR CONTRIBUTIONS

C.M. and S.C.F. designed the project. C.M. performed the experiments and analyzed the data. C.C. and S.T. provided critical reagents, including human RPE cell lines or cultures. C.M. and S.C.F. wrote the manuscript.

ACKNOWLEDGMENTS

We thank Dr. Saumil Sethna (University of Maryland, School of Medicine) for help with F-actin analyses and helpful discussions. Funding for this work was provided by NIH grant EY26215 and by the Empire State Stem Cell Fund through New York State Department of Health contract #C028504. Opinions expressed here are solely those of the authors and do not necessarily reflect those of the Empire State Stem Cell Board, the New York State Department of Health, or the State of New York.

Received: May 19, 2017
Revised: January 13, 2018
Accepted: January 15, 2018
Published: February 15, 2018

REFERENCES

Ach, T., Tolstik, E., Messinger, J.D., Zarubina, A.V., Heintzmann, R., and Curcio, C.A. (2015). Lipofuscin redistribution and loss accompanied by cytoskeletal stress in retinal pigment epithelium of eyes with age-related macular degeneration. Invest. Ophthalmol. Vis. Sci. *56*, 3242–3252.

Blenkinsop, T.A., Salero, E., Stern, J.H., and Temple, S. (2013). The culture and maintenance of functional retinal pigment epithelial monolayers from adult human eye. Methods Mol. Biol. *945*, 45–65.

Blenkinsop, T.A., Saini, J.S., Maminishkis, A., Bharti, K., Wan, Q., Banzon, T., Lotfi, M., Davis, J., Singh, D., Rizzolo, L.J., et al. (2015). Human adult retinal pigment epithelial stem cell-derived RPE monolayers exhibit key physiological characteristics of native tissue. Invest. Ophthalmol. Vis. Sci. *56*, 7085–7099.

Buchholz, D.E., Pennington, B.O., Croze, R.H., Hinman, C.R., Coffey, P.J., and Clegg, D.O. (2013). Rapid and efficient directed differentiation of human pluripotent stem cells into retinal pigmented epithelium. Stem Cells Transl. Med. *2*, 384–393.

Burgess, B.L., Abrams, T.A., Nagata, S., and Hall, M.O. (2006). MFG-E8 in the retina and retinal pigment epithelium of rat and mouse. Mol. Vis. *12*, 1437–1447.

Burstyn-Cohen, T., Lew, E.D., Traves, P.G., Burrola, P.G., Hash, J.C., and Lemke, G. (2012). Genetic dissection of TAM receptor-ligand interaction in retinal pigment epithelial cell phagocytosis. Neuron *76*, 1123–1132.

Choudhary, P., Gutteridge, A., Impey, E., Storer, R.I., Owen, R.M., Whiting, P.J., Bictash, M., and Benn, C.L. (2016). Targeting the cAMP and transforming growth factor-beta pathway increases proliferation to promote re-epithelialization of human stem cell-derived retinal pigment epithelium. Stem Cells Transl. Med. *5*, 925–937.

Croze, R.H., Buchholz, D.E., Radeke, M.J., Thi, W.J., Hu, Q., Coffey, P.J., and Clegg, D.O. (2014). ROCK inhibition extends passage of pluripotent stem cell-derived retinal pigmented epithelium. Stem Cells Transl. Med. *3*, 1066–1078.

Davis, R.J., Alam, N.M., Zhao, C., Muller, C., Saini, J.S., Blenkinsop, T.A., Mazzoni, F., Campbell, M., Borden, S.M., Charniga, C.J., et al. (2017). The developmental stage of adult human stem cell-derived retinal pigment epithelium cells influences transplant efficacy for vision rescue. Stem Cell Reports *9*, 42–49.

Edwards, R.B., and Szamier, R.B. (1977). Defective phagocytosis of isolated rod outer segments by RCS rat retinal pigment epithelium in culture. Science *197*, 1001–1003.

Feng, Q., Lu, S.J., Klimanskaya, I., Gomes, I., Kim, D., Chung, Y., Honig, G.R., Kim, K.S., and Lanza, R. (2010). Hemangioblastic derivatives from human induced pluripotent stem cells exhibit limited expansion and early senescence. Stem Cells *28*, 704–712.

Finnemann, S.C. (2003). Focal adhesion kinase signaling promotes phagocytosis of integrin-bound photoreceptors. EMBO J. *22*, 4143–4154.

Finnemann, S.C., Bonilha, V.L., Marmorstein, A.D., and Rodriguez-Boulan, E. (1997). Phagocytosis of rod outer segments by retinal pigment epithelial cells requires αvβ5 integrin for binding but not for internalization. Proc. Natl. Acad. Sci. USA *94*, 12932–12937.

Grisanti, S., and Guidry, C. (1995). Transdifferentiation of retinal pigment epithelial cells from epithelial to mesenchymal phenotype. Invest. Ophthalmol. Vis. Sci. *36*, 391–405.

Heth, C.A., and Marescalchi, P.A. (1994). Inositol triphosphate generation in cultured rat retinal pigment epithelium. Invest. Ophthalmol. Vis. Sci. *35*, 409–416.

Kokkinaki, M., Sahibzada, N., and Golestaneh, N. (2011). Human induced pluripotent stem-derived retinal pigment epithelium (RPE) cells exhibit ion transport, membrane potential, polarized vascular endothelial growth factor secretion, and gene expression pattern similar to native RPE. Stem Cells *29*, 825–835.

Lang, A.E., Schmidt, G., Schlosser, A., Hey, T.D., Larrinua, I.M., Sheets, J.J., Mannherz, H.G., and Aktories, K. (2010). *Photorhabdus*

luminescens toxins ADP-ribosylate actin and RhoA to force actin clustering. Science *327*, 1139–1142.

LaVail, M.M. (1976). Rod outer segment disk shedding in rat retina: relationship to cyclic lighting. Science *194*, 1071–1074.

Mao, Y., and Finnemann, S.C. (2012). Essential diurnal Rac1 activation during retinal phagocytosis requires αvβ5 integrin but not tyrosine kinases focal adhesion kinase or Mer tyrosine kinase. Mol. Biol. Cell *23*, 1104–1114.

Mao, Y., and Finnemann, S.C. (2013). Analysis of photoreceptor outer segment phagocytosis by RPE cells in culture. Methods Mol. Biol. *935*, 285–295.

Mao, Y., and Finnemann, S.C. (2015). Regulation of phagocytosis by Rho GTPases. Small GTPases *6*, 89–99.

Mayerson, P.L., and Hall, M.O. (1986). Rat retinal pigment epithelium shows specificity of phagocytosis in vitro. J. Cell Biol. *103*, 299–308.

Miyagishima, K.J., Wan, Q., Corneo, B., Sharma, R., Lotfi, M.R., Boles, N.C., Hua, F., Maminishkis, A., Zhang, C., Blenkinsop, T., et al. (2016). In pursuit of authenticity: induced pluripotent stem cell-derived retinal pigment epithelium for clinical applications. Stem Cells Transl. Med. *5*, 1562–1574.

Mullen, R.J., and LaVail, M.M. (1976). Inherited retinal dystrophy: primary defect in pigment epithelium determined with experimental rat chimeras. Science *192*, 799–801.

Nandrot, E.F., Anand, M., Almeida, D., Atabai, K., Sheppard, D., and Finnemann, S.C. (2007). Essential role for MFG-E8 as ligand for αvβ5 integrin in diurnal retinal phagocytosis. Proc. Natl. Acad. Sci. USA *104*, 12005–12010.

Nandrot, E.F., Kim, Y., Brodie, S.E., Huang, X., Sheppard, D., and Finnemann, S.C. (2004). Loss of synchronized retinal phagocytosis and age-related blindness in mice lacking αvβ5 integrin. J. Exp. Med. *200*, 1539–1545.

Nandrot, E.F., Silva, K.E., Scelfo, C., and Finnemann, S.C. (2012). Retinal pigment epithelial cells use a MerTK-dependent mechanism to limit the phagocytic particle binding activity of αvβ5 integrin. Biol. Cell *104*, 326–341.

Parinot, C., Rieu, Q., Chatagnon, J., Finnemann, S.C., and Nandrot, E.F. (2014). Large-scale purification of porcine or bovine photoreceptor outer segments for phagocytosis assays on retinal pigment epithelial cells. J. Vis. Exp. *94*. https://doi.org/10.3791/52100.

Pilgrim, M.G., Lengyel, I., Lanzirotti, A., Newville, M., Fearn, S., Emri, E., Knowles, J.C., Messinger, J.D., Read, R.W., Guidry, C., and Curcio, C.A. (2017). Subretinal pigment epithelial deposition of drusen components including hydroxyapatite in a primary cell culture model. Invest. Ophthalmol. Vis. Sci. *58*, 708–719.

Salero, E., Blenkinsop, T.A., Corneo, B., Harris, A., Rabin, D., Stern, J.H., and Temple, S. (2012). Adult human RPE can be activated into a multipotent stem cell that produces mesenchymal derivatives. Cell Stem Cell *10*, 88–95.

Singh, R., Phillips, M.J., Kuai, D., Meyer, J., Martin, J.M., Smith, M.A., Perez, E.T., Shen, W., Wallace, K.A., Capowski, E.E., et al. (2013). Functional analysis of serially expanded human iPS cell-derived RPE cultures. Invest. Ophthalmol. Vis. Sci. *54*, 6767–6778.

Strauss, O. (2005). The retinal pigment epithelium in visual function. Physiol. Rev. *85*, 845–881.

Tamiya, S., Liu, L., and Kaplan, H.J. (2010). Epithelial-mesenchymal transition and proliferation of retinal pigment epithelial cells initiated upon loss of cell-cell contact. Invest. Ophthalmol. Vis. Sci. *51*, 2755–2763.

Westenskow, P.D., Moreno, S.K., Krohne, T.U., Kurihara, T., Zhu, S., Zhang, Z.N., Zhao, T., Xu, Y., Ding, S., and Friedlander, M. (2012). Using flow cytometry to compare the dynamics of photoreceptor outer segment phagocytosis in iPS-derived RPE cells. Invest. Ophthalmol. Vis. Sci. *53*, 6282–6290.

Young, R.W. (1967). The renewal of photoreceptor cell outer segments. J. Cell Biol. *33*, 61–72.

Young, R.W., and Bok, D. (1969). Participation of the retinal pigment epithelium in the rod outer segment renewal process. J. Cell Biol. *42*, 392–403.

Stem Cell Reports, Volume *10*

Supplemental Information

Quantified F-Actin Morphology Is Predictive of Phagocytic Capacity of Stem Cell-Derived Retinal Pigment Epithelium

Claudia Müller, Carol Charniga, Sally Temple, and Silvia C. Finnemann

Supplementary Table 1. Information on tissue donors, tissue procurement, and RPE cell yield.

RPE line	Age	Cause of death	Time death to enucleation (h)	Time death to isolation of cells (h)	RPE cell yield (million)
1	78	Lung CA + metastasis	6.7	30.5	1.07
2	53	Breast CA + metastasis	7.1	23.0	2.03
3	76	Respiratory failure	4.8	34.0	1.25
4	74	Arteriosclerotic CVD	16.0	38.8	1 globe only: 1.02
5	67	Cardiac arrest	6.4	24.5	2.7
6	67	Cardiac arrest	5.4	39.0	3.4
7	73	Myocardial infarct	7.0	29.8	1 globe only: 1.34
8	70	Cardiopulmonary arrest	6.0	22.0	3.18